Direct Observation of Magnetic Transitions in a Nickel(II) Complex with Large Anisotropy

Chelsea N. Widener,^a Alexandria N. Bone,^a Mykhaylo Ozerov,^b Rachael Richardson,^c Zhengguang Lu,^b Komalavalli Thirunavukkuarasu,^c Dmitry Smirnov,^b Xue-Tai Chen,^d Zi-Ling Xue^{a,*}

- ^a Department of Chemistry, University of Tennessee, Knoxville, Tennessee 37996, United States
- ^b National High Magnetic Field Laboratory, Tallahassee, Florida 32310, United States
- ^c Department of Physics, Florida A&M University, Tallahassee, Florida 32307, United States
- ^d State Key Laboratory of Coordination Chemistry, School of Chemistry and Chemical Engineering, Nanjing University, Nanjing 210023, China

Abstract

Trigonal bipyramidal Ni(II) complex [Ni(Me₆tren)Cl](ClO₄) (**1**, Me₆tren = tris[2-(dimethylamino)ethyl]amine) has recently been shown by Ruamps and coworkers to possess large, uniaxial magnetic anisotropy (*J. Am. Chem. Soc.* **2013**, *135*, 3017). Their HF-EPR studies gave rhombic zero-field-splitting (ZFS) parameter E = 1.56(5) cm⁻¹ for **1**. However, the axial ZFS parameter D has not been determined. We have used far-IR magnetic spectroscopy (FIRMS) at 0-17.5 T and 5 K to probe the magnetic transitions between the $M_S = \pm 1$ and $M_S = 0$ states of the ground spin state S = 1 in **1**. Direct observation of the transitions between Zeeman-split states in FIRMS give axial ZFS parameter D = -110.7(3) cm⁻¹. Hirshfeld surface analysis of the crystal structure of **1** has **Date received**: 2020-mm-dd. **Date revised**: **Supported by** U.S. National Science Foundation (No. CHE-1633870, CHE-1900296) ***Corresponding author** Zi-Ling Xue. **Email**: xue@utk.edu

been performed, revealing the interactions between the cation and anion in a molecule of **1** as well as among the molecules of **1** in crystals.

Introduction

Magnetic properties of transition metal complexes have been actively studied recently, in part to understand the fundamental nature of the complexes and in part to probe their potential applications as single-molecule magnets (SMMs) and chemical qubits. [1-19] For paramagnetic compounds with $S \ge 1$ and quenched orbital angular momenta, the ground electronic states of the compounds are split (zero-field splitting or ZFS) from second-order spin-orbital coupling involving the ground electronic states. [1-17] The degree of the magnetic anisotropy is measured by axial (D) and rhombic (E) ZFS parameters. [15] Ni(II) complexes displaying SMM properties have been reported. [20-25] The d⁸ complex in the current study, [Ni(Me₆tren)Cl](ClO₄) (1), contains a trigonal bipyramidal cation (Fig. 1). In the trigonal crystal structure of 1 (E) E space group, No. 161), the [Ni(Me₆tren)Cl]+ cation sits on a 3-fold axis (Fig. 1b). Thus, the crystallographic point group symmetry of the metal site (paramagnetic center) is axial and 3-fold. In other words, the (E, E) directions are degenerate. However, as discussed below, Jahn-Teller distortion leads to the breakup of the degeneracy.

The d orbitals in the Ni(II) ion in **1** are split by the ligand field into three sets as shown in Fig. 1-Right. There are three electrons in the middle level, a degenerate set (e). Jahn-Teller distortion of the molecule of **1** to lower the energy leads to the splitting of the degenerate orbitals, as shown in Fig. 1-Right. With such five non-degenerate d orbitals in the Jahn-Teller distorted cation [Ni(Me₆tren)CI]⁺, the orbital angular

momentum is quenched. The two unpaired electrons in the Ni(II) complex (S = 1) undergo second-order spin-orbital coupling with excited electronic states, leading to zero-field splitting (ZFS) of the triplet ground electronic state 3A_2 into the $M_S = 0$ and doublet $M_S = \pm 1$ states. When the axial parameter D < 0, as in 1, the molecule has an easy axis of magnetization in the z direction which is typically assumed to be parallel to the C_3 axis. When D > 0, the molecule possesses an easy plane of magnetization in the x,y direction. In the Jahn-Teller distorted [Ni(Me₆tren)Cl]⁺, there is additional splitting of the degenerate $M_S = \pm 1$ states by the rhombic (E) parameter (Fig. 2). The determination of the ZFS parameters is vital to understanding magnetic properties of the complex. [1-17]

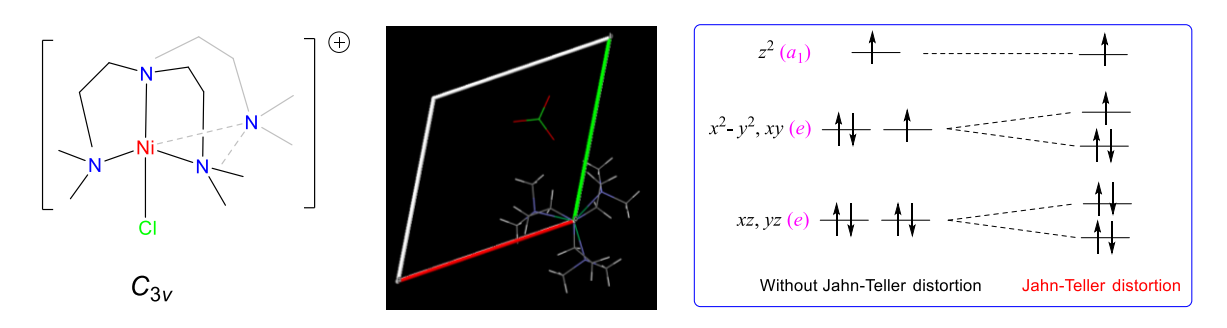


Fig. 1. (Left) [Ni(Me₆tren)Cl]⁺ cation in **1** with local $C_{3\nu}$ symmetry. (Middle) View of the cation and anion in **1** looking down the crystallographic c axis, showing that the cation is on a C_3 axis. a axis: red; b axis: green. (Right) Splitting of the d orbitals in the [Ni(Me₆tren)Cl]⁺ cation. The a_1 and e symbols refer to the symmetries of the d orbitals in the $C_{3\nu}$ point group.

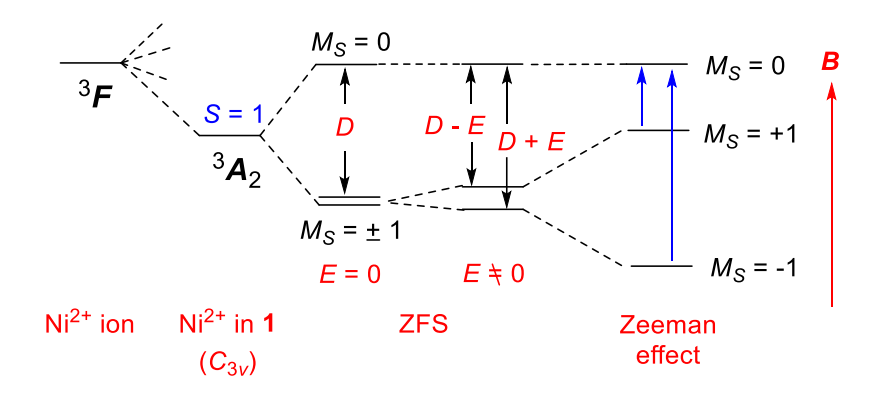


Fig. 2. Ground-state triplet levels in high-spin, d^8 complexes with C_{3v} symmetry. $E \neq 0$ leads to additional splitting of the degenerate $M_S = \pm 1$ states. Under magnetic fields, the Zeeman effect shifts the $M_S = -1$ and $M_S = +1$ states. The $M_S = -1 \rightarrow 0$ and $M_S = +1 \rightarrow 0$ transitions at low temperatures are allowed.

Magnetometry (or direct-current susceptibility magnetic measurement) is often employed to estimate the ZFS in metal complexes, [4] even though this is an indirect method based on essentially a multi-parameter fit of susceptibility and magnetization data by the spin-Hamiltonian. In addition, the sign of D is often not easily determined by magnetometry. High-frequency and high-field electron paramagnetic resonance (HF-EPR) has been used to study ZFS typically up to ~33 cm⁻¹ (1 THz).[4, 26] Ruamps and coworkers have used HF-EPR to probe a single crystal of [Ni(Me₆tren)Cl](ClO₄) (1) to give E = 1.56(5) cm⁻¹ and $g_z = 2.34(7)$.[27] The D value in 1 was estimated to be between -120 and -180 cm⁻¹.[27] A subsequent semiempirical model study of the Ni(II) ion in 1 has been conducted to analyze the large ZFS.[28]

FIRMS (far-IR magneto spectroscopy) is a direct technique to probe transitions such as those among ZFS states in transition metal complexes and magnetic transitions in f-element complexes.^[4, 31-40] It involves the use of magnetic fields in probing a sample

by far-IR spectroscopy.^[29-33] Earlier work by Brackett and Richards demonstrated that transitions among the ZFS states are magnetic-dipole allowed, making these transitions observable in far-IR.^[29-30] In FIRMS, the sample is placed in variable magnetic fields. The Zeeman effect on the magnetic levels shifts the magnetic peaks in FIRMS, thus helping reveal magnetic transitions in metal complexes that are too large to be measured by HF-EPR.

Understanding intermolecular interactions helps probe whether single-molecule magnets (SMMs) behave truly as individual molecules/magnets or the interactions among the molecules in the crystals of the compounds contribute to the observed properties. Hirshfeld surface analysis is a newly developed method to study interactions of an individual molecule with its nearest neighbor molecules. [41-44] It is a simple approach of mapping void space in molecular crystals. A Hirshfeld surface is an isosurface calculated from the weight function $w(\mathbf{r})$ of the sum of spherical atom electron densities in Eq. 1:

$$w(\mathbf{r}) = \frac{\rho_{promolecule}(\mathbf{r})}{\rho_{procrystal}(\mathbf{r})} = \sum_{A \in molecule} \rho_A(\mathbf{r}) / \sum_{A \in crystal} \rho_A(\mathbf{r})$$
(Eq. 1)

where $\rho_{\text{promolecule}}(\mathbf{r})$ = sum of the molecular electron density over the atoms in the molecule of interest (the promolecule); $\rho_{\text{procrystal}}(\mathbf{r})$ = similar sum over the crystal (the procrystal). [41-44]

The Hirshfeld surface leads to a visual 3-*D* representation of the intermolecular close contacts in the crystal and computations of surface areas and volumes of the

voids in the crystals.^[45] Hirshfeld surface analysis is an excellent method to study molecular environment and interactions of compounds independent of the overall space group symmetry. We recently used the Hirshfeld surface analyses to study structures of metalloporphyrins Fe(TPP)CI,^[46] M(TPP)(NO) (M = Fe, Co),^[46] and Mn(TPP)X•solvent (X = Br, solvent = CHCl₃, CH₂Cl₂; X = I, solvent = CHCl₃, CDCl₃ and 1.5CHCl₃).^[47] These analyses show that intermolecular interactions contribute significantly to structural disorders of Fe(TPP)Cl and phase changes in M(TPP)(NO) (M = Fe, Co).^[46]

In the current work, we have used FIRMS at 5 K to probe the ZFS transitions in **1**. By using E = 1.56 cm⁻¹ from the earlier HF-EPR studies, [27] fitting the far-IR data gives D = -110.7(3) cm⁻¹. Hirshfeld surface analyses of the crystal structure of **1** show the interactions among the ions (cations [Ni(Me₆tren)Cl]⁺ and anions ClO₄⁻) in the crystalline solid of **1**.

Experimental

Sample of [Ni(Me₆tren)Cl](ClO₄) (1) was prepared by the literature method. [27]

Far-IR studies

Far-IR spectroscopic studies were conducted at the National High Magnetic Field Laboratory (NHMFL) at Florida State University. Transmittance far-IR spectra were collected using the powdered samples. The samples were mixed with eicosane and pressed into pellets that were approximately 1 mm thick. Spectra were collected at 5 K using a Bruker Vertex 80v FT-IR spectrometer coupled with a superconducting magnet (SCM 3) with fields up to 17.5 T.

Raman studies

Raman samples were prepared with unoriented single crystals of **1**. Data were collected by a backscattering Faraday geometry using a 532 nm laser at an 18 T superconducting magnet (SCM 2) or at a 14 T SCM in the Electron Magnetic Resonance (EMR) in the DC Field facility at NHMFL. Crystals of samples were cooled at 1.5 K (18 T). Collected scattered light was guided via an optical fiber to a spectrometer equipped with a liquid nitrogen-cooled CCD camera.

Hirshfeld surface calculations

Hirshfeld surfaces were calculated using CrystalExplorer (version 17) software from the crystal-structure coordinates supplied in the format of crystallographic information file (CIF).^[48] The reported X-ray CIF file of **1** at 100(1) K (CCDC 893397)^[27] was used. Hirshfeld surfaces were calculated at an isovalue of 0.5 e au⁻³. Void volumes were calculated using an isovalue of 0.002 e au⁻³.^[45]

Results and discussion

FIRMS studies

The zero-field splitting in Ni compound was studied by the far-infrared magneto-spectroscopy (FIRMS) technique. This technique employs the Fourier-transform spectrometer to measure the magnetic response from the sample in the frequency domain (down to 20 cm⁻¹) while the magnetic field is fixed [in contrast to the electron paramagnetic resonance (EPR), where the frequency is fixed and magnetic field is swept]. The sample is placed in a cryostat equipped by a vertical bore superconducting

magnet and coupled to the spectrometer through the evacuated optical beam line. In this manner, the intensity of far-IR radiation transmitted through the sample was recorded with magnetic fields (up to 17 T) and at temperature of 4.5 K. In all measurements, the magnetic field is applied in Voigt geometry (magnetic field perpendicular to the wave vector of the radiation). All samples were a mixture of the eicosane matrix with microcrystalline powders and different trials were made for a variety of mixture ratios and sample thicknesses. The FIRMS spectra and a contour plot are shown in Fig. 3. Transmission of 1 normalized to the zero-field spectrum T_B / T_0 at 1-17 T is given in Fig. S1 in Supporting Information.

For the interpretation of far-IR data of the Ni compound 1, the measured data are presented in terms of normalized transmission. The transmission spectrum measured at each magnetic field was normalized to the reference spectrum computed as an averaging of spectra for all magnetic fields and removing outliers points. Such normalization shows up field-induced features masked at the original spectra due to the overlapping of the feature with phononic or intramolecular vibrational excitations. The quantitative contribution of magnetic excitations to absolute absorption of the sample is determined by the decrease in the normalized transmission. Therefore, this experimentally accessible quantity allows direct access to the transition intensity between field-dependent spin energy levels.

A simulation in-house program was written in Matlab for analysis of the magnetic field dependence of normalized transmission. The program is based on the *EasySpin* toolbox, allowing the calculations of the transition matrix element of the magnetic dipole transitions. Originally developed for the simulating and fitting a wide range of EPR

spectra, the *EasySpin* toolbox provides a frequency-domain simulation capabilities.^[49] The simulation is performed for single magnetic center with the S = 1 spin Hamiltonian

$$\widehat{H} = \mu_B \vec{B} \cdot \hat{g} \cdot \vec{S} + \vec{S} \cdot \widehat{D} \cdot \vec{S}$$
 (Eq. 2)

where μ_B is Bohr magneton constant, \vec{B} is magnetic field vector, $\vec{\mathcal{S}}$ is vector spin

operator, and
$$\hat{g}=\begin{pmatrix}g_x&0&0\\0&g_y&0\\0&0&g_z\end{pmatrix}$$
 is Landé tensors of the electron spin, and $\widehat{D}=$

$$\begin{pmatrix} -\frac{1}{3}D + E & 0 & 0 \\ 0 & -\frac{1}{3}D - E & 0 \\ 0 & 0 & -\frac{2}{3}D \end{pmatrix}$$
 is the ZFS tensor expressed by commonly used D and

E zero-field splitting parameters. The input parameters $g_x = g_y = 2.4$, $g_z = 2.34$ and E = 1.56 cm⁻¹ were fixed and taken from Ref. 27. D was only one variable parameter. To take into account the random orientation of the microcrystallites (i.e., magnetic center) in a powder, integration over the different directions was implemented using a standard option of the "pepper" function in the EasySpin toolbox. The final absorption intensity spectra are obtained by introducing the line broadening parameter onto the calculated transition probabilities. The results of the fittings are shown in Fig. 3-Bottom. The simulations yielded D = -110.7(3) cm⁻¹.

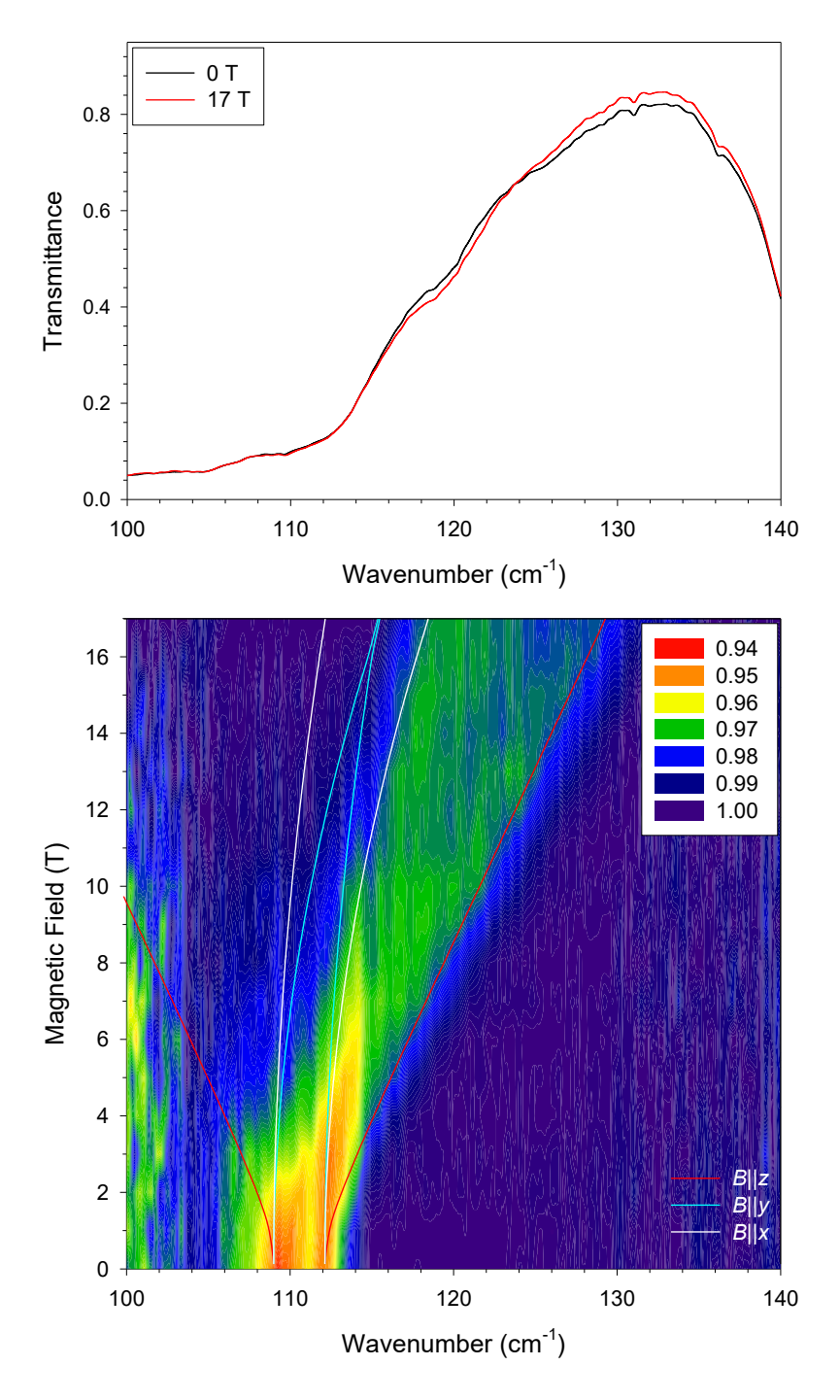


Fig. 3. (Top) Far-IR spectra of **1** at 0 and 17 T magnetic fields. (Bottom) Contour maps in 0–17 T magnetic fields. Fittings by the *EasySpin* program for the Zeeman splittings in the B||x, B||y and B||z directions.

Raman spectra

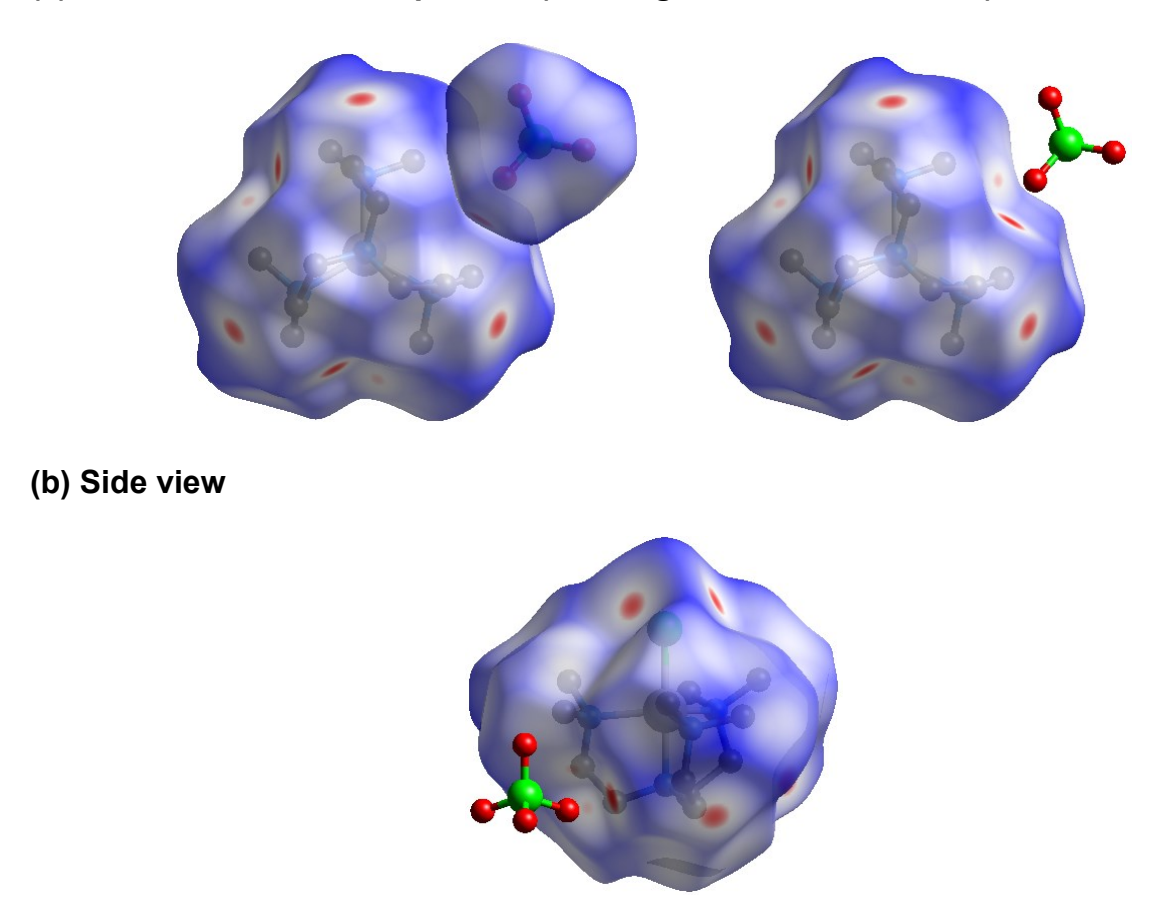
Raman spectra of a cut crystal of **1** show no magnetic feature (Fig. S2). The ZFS transition in the range of the magnetic feature in far-IR (Fig. 3) was not observed in Raman spectra. Although the ZFS transition was not observed in Raman spectra of Co(acac)₂(H₂O)₂ (acac⁻ = acetylacetonate), the spin-phonon coupling of the ZFS transition and nearby Raman-active phonons allow the ZFS transitions to obtain the intensities of the phonon transitions, leading to the observation of both ZFS and phonon peaks.^[32] However, there is apparently no Raman-active phonons near the ZFS transition in the Ni(II) complex **1** here (Fig. S2).

Hirshfeld surface analyses

Hirshfeld surface of [Ni(Me₆tren)Cl](ClO₄) (1) at 100(1) K is presented in Fig. 4 with views from the top, bottom and side of the cation [Ni(Me₆tren)Cl]⁺. The red-white-blue coloring scheme in Fig. 4 demonstrates decreasing contacts. Sites of close contacts are shown in red dots. Although there is close contact involving the "top" N atom on the C₃ axis, the void between two [2-(dimethylamino)ethyl]amine "arms" involves close contact with the anion ClO₄⁻, as revealed in the top and side views in Fig. 4a-b. The bottom views (Fig. 4c) show that Cl⁻ ligand is in close contact with the H atoms of the methyl groups on the neighboring molecules. Additional views of the Hirshfeld surface with the packing diagram are given in Figs. S3 and S4 of Supporting Information.

The volumes and surface areas of the cation, anion ClO₄- and the void in the crystal of **1** from the Hirshfeld surface analyses are given in Table 1.

(a) Hirshfeld surface – Top views (Looking down the N-Ni bond)



(c) Bottom views (Looking down the CI-Ni bond) with a packing diagram

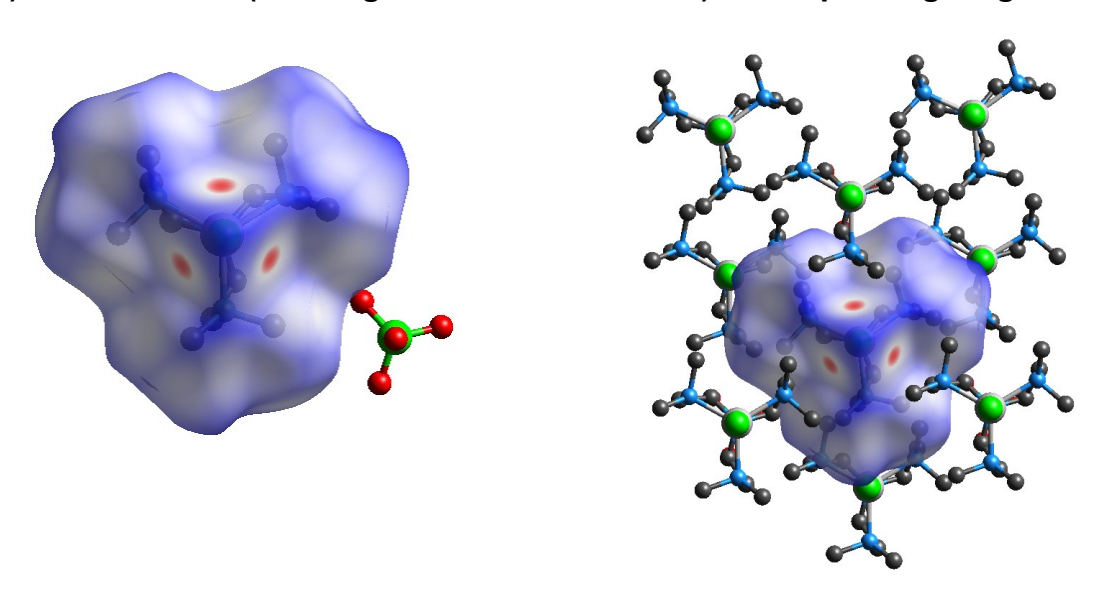


Fig. 4. Hirshfeld surface of **1** showing normalized close distances of the pro-molecule at 100(1) K. Semi-transparent view reveals the enclosed cation and anion.

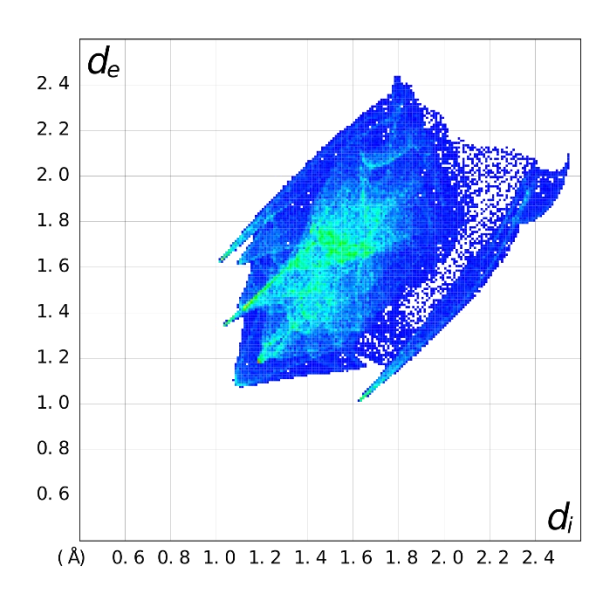
Table 1. Volumes and surface areas from Hirshfeld surface analyses

	Volume (nm³)	Surface area (nm²)
[Ni(Me ₆ tren)Cl] ⁺ cation	0.38257	2.9487
CIO ₄ - anion	0.07177	0.9057
Void	0.29876	9.5627

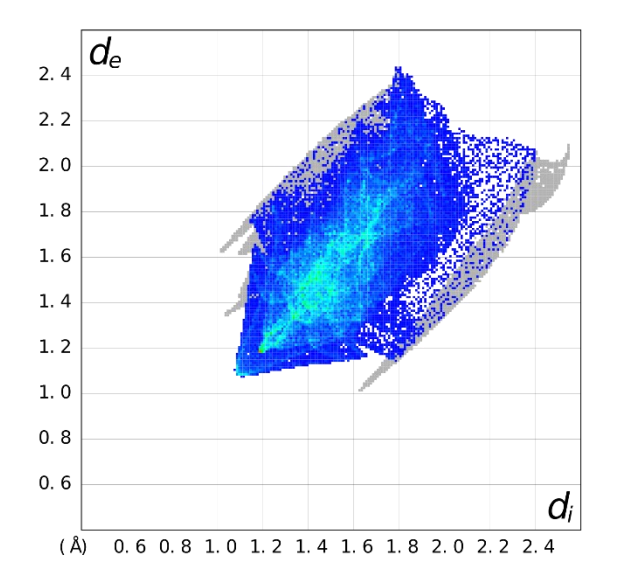
Fingerprint plots, such as those in Fig. 5 derived from the Hirshfeld surface, [50] provide a "fingerprint" of the intermolecular interactions in the crystal.[41-45] They give a visual summary of the frequency of d_e and d_i combinations across the surface of a molecule.[50] de is the distance from the surface to the nearest nucleus external to the surface. di is the distance from the surface to the nearest nucleus internal to the surface. [43, 51] Each point on the 2D graph (Fig. 5) represents a bin of width 0.01 Å in de and di with color indicating the fraction of surface points in that bin: blue (relatively few points), green (moderate fraction) and red (many points). [43] As Spackman and coworkers indicated, the de and di range varies considerably across the Hirshfeld surface, and the change depends on the atoms in the molecule (i.e., size dependence) and the type of intermolecular interaction involved (i.e., interaction dependence).^[51] Fig. 5 shows that the closest contacts correspond to the minimum values of $d_e + d_i$ are: 0.22 nm for H···H (Fig. 5b); 0.26 nm for Cl···H (Fig. 5c); 0.24 nm for O···H (Fig. 5d). The H···H contacts, as like···like contacts are featured more along the diagonal (Fig. 5b). [50] The 'wings' in Fig. 5a are due to the Cl...H (Fig. 5c) and O...H interactions (Fig. 5d).

As indicated earlier, Hirshfed surface analyses here show the interactions of ions in the crystalline solid of 1.

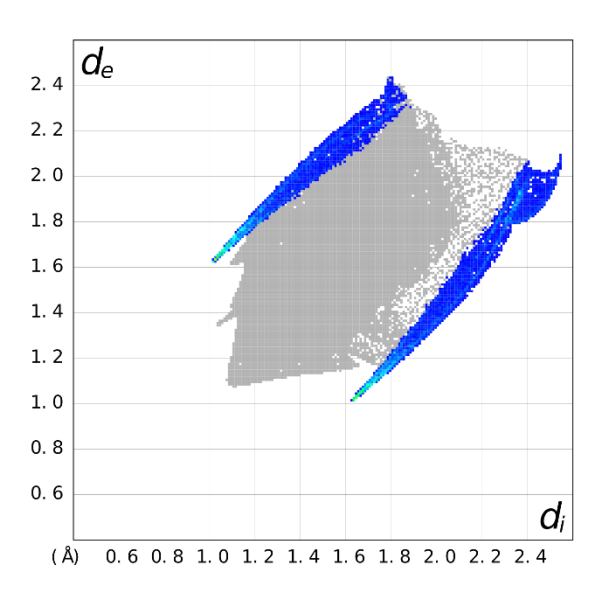
(a) All contacts below



(b) H-H contacts (blue-green) below



(c) CI-H contacts (blue-green) below



(d) O-H contacts (blue-green) below

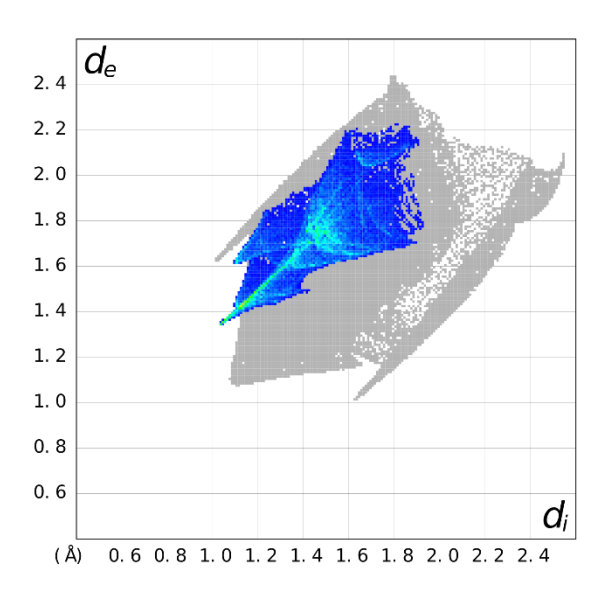


Fig. 5. Hirshfeld fingerprint plots.

In summary, the current work led to direct observation of the transitions between ZFS states in **1** by FIRMS, yielding the axial ZFS parameter D = -110.7(3) cm⁻¹. Thus, both ZFS parameters, D and the rhombic E = 1.56(5) cm⁻¹ from earlier HF-EPR work, [27]

are obtained from the combined spectroscopic studies. Hirshfeld surface analyses of the crystal structure of **1** at 100(1) K give volumes and surface areas of the cation [Ni(Me₆tren)Cl]⁺, anion ClO₄⁻ and void in **1**. In addition, "fingerprints" of the intermolecular interactions reveal the intermolecular interactions in the crystal.

Supporting Information

Normalized Far-IR transmission spectra, Raman spectra, and contour plot and additional views of the Hirshfeld surface of **1**.

Acknowledgement

The authors thank financial support by the U.S. National Science Foundation (CHE-1633870 and CHE-1900296 to Z-L.X.). Part of this work was done at the National High Magnetic Field Laboratory, which is supported by U.S. National Science Foundation through Cooperative Agreement DMR-1644779 and the State of Florida.

摘要

Ruamps和同事最近发现三角双锥构型的Ni(II) 络合物 [Ni(Mestren)Cl](ClO4) ($\mathbf{1}$, Mestren = tris[2-(dimethylamino)ethyl]amine) 具有大的单轴磁各向异性 (J. Am. Chem. Soc. $\mathbf{2013}$, 135, 3017)。他们利用HF-EPR研究获得横向零场分裂 (ZFS) 参数E=1.56(5) cm⁻¹, 但未能确定轴向零场分裂参数D。在本工作中,我们利用0-17.5 T和5 K的变磁场远红外光谱 (FIRMS) 来检测自旋基态S=1中的 $M_S=\pm1$ 和 $M_S=0$ 态之间的磁跃迁。在FIRMS中直接观察到Zeeman分裂态之间的跃迁,得出轴向ZFS参数D=-110.7(3) cm⁻¹。我们对 $\mathbf{1}$ 的晶体结构进行了Hirshfeld表面分析,揭示了 $\mathbf{1}$ 分子中的阳离子与阴离子之间以

及分子之间的相互作用。

References

- [1] Benelli C and Gatteschi D. *Introduction to Molecular Magnetism*. Weinheim: Wiley-VCH, **2015**: 217-237.
- [2] Frost J M, Harriman K L M, Murugesu M. Chem. Sci., 2016, 7: 2470-2491.
- [3] Layfield R A. Organometallics, 2014, 33: 1084-1099.
- [4] Krzystek J and Telser J. Dalton Trans., 2016, 45: 16751-16763.
- [5] McInnes E J L and Winpenny R E P. Comprehensive Inorganic Chemistry II.

 Amsterdam: Elsevier, **2013**: 371-395.
- [6] Neese F and Pantazis D A. Faraday Discuss., 2011, 148: 229-238.
- [7] Gao S. Molecular Nanomagnets and Related Phenomena. Heidelberg: Springer, 2015: 1-460.
- [8] Zhang P, Zhang L, Tang J. *Dalton Trans.*, **2015, 44:** 3923-3929.
- [9] Liu J-L, Chen Y-C, Tong M-L. Chem. Soc. Rev., 2018, 47: 2431-2453.
- [10] Craig G A and Murrie M. Chem. Soc. Rev., 2015, 44: 2135-2147.
- [11] Rinehart J D and Long J R. *Chem. Sci.*, **2011, 2**: 2078-2085.
- [12] Gatteschi D, Sessoli R. Angew. Chem. Int. Ed., 2003, 42: 268-297.
- [13] Demir S, Jeon I-R, Harris T D, et al. Coord. Chem. Rev., 2015, 289: 149-176.
- [14] Dey M and Gogoi N. *Angew. Chem. Int. Ed.*, **2013, 52:** 12780-12782.
- [15] Boča R. Coord. Chem. Rev., 2004, 248: 757-815.
- [16] Shatruk M, Gómez-Coca S, Dunbar K R. *Molecular Magnetic Materials: Concepts and Applications*. Weinheim: Wiley-VCH, **2017**: 29-77.

- [17] Yamashita M and Katoh K. *Molecular Magnetic Materials: Concepts and Applications*. Weinheim: Wiley-VCH, **2017:** 79-101.
- [18] Gatteschi D, Sessoli R, Villain J. Molecular Nanomagnets. Oxford: Oxford University Press, 2006: 1-317.
- [19] Stavretis S E, Mamontov E, Xue Z-L, et al. *Phys. Chem. Chem. Phys.*, **2018, 20**: 21119-21126.
- [20] Marriott K E R, Bhaskaran L, Murrie M, et al. Chem. Sci., 2015, 6: 6823-6828.
- [21] Miklovič J, Valigura D, Titiš J, et al. *Dalton Trans.*, **2015, 44:** 12484-12487.
- [22] Lomjanský D, Moncol J, Boča R, et al. Chem. Commun., 2017, 53: 6930-6932.
- [23] Craig G A, Sarkar A, Murrie M, et al. Chem. Sci., 2018, 9: 1551-1559.
- [24] Titiš J, Rajnák C, Boča R, et al. *Dalton Trans.*, **2018, 47:** 7879-7882.
- [25] Titiš J, Chrenková V, Boča R, et al. *Dalton Trans.*, **2019**, **48**: 11647-11650.
- [26] Chen L, Wang J, Xue Z-L, et al. J. Am. Chem. Soc., 2014, 136: 12213-12216.
- [27] Ruamps R, Maurice R, Guihéry N, et al. J. Am. Chem. Soc., 2013, 135: 3017-3026.
- [28] Rudowicz C, Açıkgöz M, Gnutek P. J. Magn. Magn. Mater., 2017, 434: 56-61.
- [29] Brackett G C. Far-Infrared Magnetic Resonance in Fe(III) and Mn(III) Porphyrins,

 Myoglobin, Hemoglobin, Ferrichrome A, and Fe(III) Dithiocarbamates, Ph.D.

 dissertation. Berkeley: University of California Berkeley, **1970**.
- [30] Brackett G C, Richards P L, Caughey W S. J. Chem. Phys., **1971, 54:** 4383-4401.
- [31] Rechkemmer Y, Breitgoff F D, van Slageren J, et al. *Nat. Commun.*, **2016, 7**: 10467.
- [32] Moseley D H, Stavretis S E, Xue Z-L, et al. Nat. Commun., 2018, 9: 2572.
- [33] Stavretis S E, Moseley D H, Xue Z-L, et al. Chem. Eur. J., 2019, 25: 15846-15857.

- [34] Ray K, Begum A, Wieghardt K, et al. *J. Am. Chem. Soc.*, **2005, 127:** 4403-4415.
- [35] Rechkemmer Y, Fischer J E, van Slageren J, et al. *J. Am. Chem. Soc.*, **2015, 137:** 13114-13120.
- [36] Bunting P C, Atanasov M, Long J R, et al. Science, 2018, 362: eaat7319.
- [37] Jiang S-D, Maganas D, Kyritsis P, et al. J. Am. Chem. Soc., 2015, 137: 12923-12928.
- [38] Świtlicka A, Machura B, Ozerov M, et al. Inorg. Chem., 2018, 57: 12740-12755.
- [39] Hay M A, Sarkar A, Murrie M. Chem. Sci., 2019, 10: 6354-6361.
- [40] Haas S. Far-infrared spectroscopy of lanthanide-based molecular magnetic materials, Ph.D. dissertation. Stuttgart: University of Stuttgart, **2015**.
- [41] McKinnon J J, Jayatilaka D, Spackman M A. Chem. Commun., 2007, 37: 3814-3816.
- [42] Spackman M A and Jayatilaka D. CrystEngComm, 2009, 11: 19-32.
- [43] Spackman M A and McKinnon J J. CrystEngComm, 2002, 4: 378-392.
- [44] McKinnon J J, Spackman M A, Mitchell A S. *Acta Cryst B*, **2004, 60**: 627-668.
- [45] Turner M J, McKinnon J J, Spackman M A, et al. *CrystEngComm*, **2011, 13:** 1804-1813.
- [46] Hunter S C, Smith B A, Xue Z-L, et al. Inorg. Chem., 2014, 53: 11552-11562.
- [47] Bone A N, Stavretis S E, Xue Z-L, et al. *Polyhedron*, **2020.** *Accepted for publication*.
- [48] Turner M J, McKinnon J J, Wolff S K, Grimwood D J, Spackman P R, Jayatilaka D, Spackman M A. CrystalExplorer17.
- [49] Stoll S and Schweiger A. J. Magn. Reson., **2006**, **178**: 42-55.

[50] Fingerprint plots; Website:

http://crystalexplorer.scb.uwa.edu.au/wiki/index.php/Fingerprint_Plots.

[51] Hirshfeld surface properties; Website:

http://crystalexplorer.scb.uwa.edu.au/wiki/index.php/Surface_Properties.